T. L. Naing, T. O. Rocheleau, Z. Ren, E. Alon, and C. T.-C. Nguyen, "Vibration-Insensitive 61-MHz Micromechanical Disk Reference Oscillator," *Proceedings*, 2012 IEEE Int. Frequency Control Symp., Baltimore Maryland, May 21-24, 2012, pp. 276-281.

Vibration-Insensitive 61-MHz Micromechanical Disk Reference Oscillator

Thura Lin Naing, Tristan O. Rocheleau, Zeying Ren, Elad Alon, and Clark T.-C. Nguyen
Dept. of Electrical Engineering and Computer Sciences
University of California at Berkeley
Berkeley, CA 94720 USA
E-mail: thura@eecs.berkeley.edu

Abstract— A low phase noise oscillator referenced to a 61-MHz vibrating wine-glass disk resonator with anchor-isolating supports designed to suppress microphonics has posted (without any compensation) a measured acceleration sensitivity at least as good as Γ ~0.2ppb/g for vibration frequencies up to 2kHz and in all directions, yielding a vector magnitude $|\vec{\Gamma}|$ less than 0.5ppb/g. Remarkably, this result is at least 30 times better than previous work using a similar wine-glass disk resonator and is the best mark among MEMS-based oscillators to date, including those aided by feedback compensation circuits. It is also more than an order of magnitude better than an off-the-shelf crystal oscillator and is now comparable with low sensitivity oven-controlled crystal oscillators (OCXO's). Such low sensitivity to environmental vibration by a tiny uncompensated MEMS-based oscillator is expected to enable harsh environment and military applications that require stable and compact reference oscillators.

***Keywords*—MEMS, oscillator, microphonics, acceleration sensitivity, vibration sensitivity, micromechanical, wine-glass disk, quality factor, resonator, RF MEMS.**

I. Introduction

The performance of electronic circuits and systems used in wireless communications depends strongly on the accuracy and stability of timing and frequency reference oscillators. For example, communication between a wireless receiver and a far-away transmitter can often be masked by the noise, i.e., short-term instability, of another transmitter closer to the receiver. From a practical standpoint, there are three main ways to improve the short-term frequency stability of an oscillator that limits through gentle nonlinearity (e.g., an automatic level control loop) [1]: 1) increase its loop signal power; 2) increase the quality factor (Q) of its resonator; and 3) suppress its noise.

Using these guidelines, previous 61-MHz micromechanical wine-glass disk oscillators, when divided down to 13MHz, have achieved phase noise marks of -138 and -151dBc/Hz at 1kHz and far-from-carrier offset frequencies, respectively, both of which satisfy the Global System for Mobile Communications (GSM) reference oscillator standard [2]. Unfortunately, for many applications simply lowering electronics-induced phase noise is only half the battle. In particular, phase noise degrades dramatically when an oscillator experiences vibration. Vibration, of course, is everywhere, from buildings with typical accelerations of 0.02g, to missiles with accelerations up to 100g.

Much of the described work was supported by DARPA.

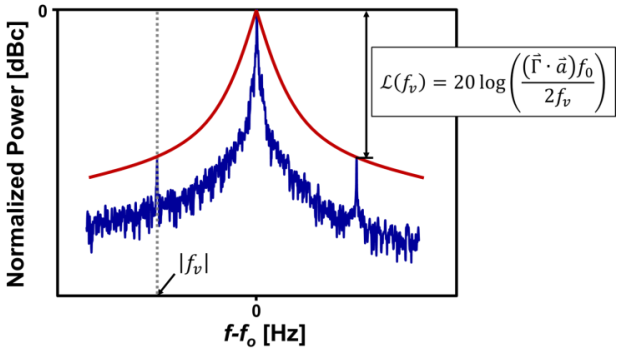

Fig. 1: A typical oscillator output power spectrum in the presence of vibration with frequency f_v. The ratio between the sidebands and output characterizes the acceleration sensitivity of the oscillator. The red curve illustrates a broad spectrum of increased phase noise under random vibration.

Fig. 1 illustrates the influence on the output power spectrum typically seen for an oscillator experiencing vibration. Here, vibration induces spikes at frequencies offset from the carrier by the vibration frequency, f_v. Normally, vibration occurs randomly at all frequencies up to a few kHz, so instead of spikes of added noise, a broad spectrum of increased phase noise often ensures, as illustrated by the red curve in Fig. 1. In traditional quartz-based oscillators, the primary cause of this acceleration sensitivity is often changes in stress at the mounting points of the crystal.

In this work, a low phase noise oscillator referenced to a 61-MHz vibrating wine-glass disk resonator is presented that posts a measured acceleration sensitivity at least as good as Γ ~0.2ppb/g for vibration frequencies up to 2kHz and in all directions, yielding a vector magnitude $|\vec{\Gamma}|$ less than 0.5ppb/g. This impressive result is the best mark to date among MEMS-based oscillators, including those aided by feedback compensation circuits; is more than an order of magnitude better than an off-the-shelf crystal oscillator; and is now comparable with low acceeration sensitivity oven-controlled crystal oscillators (OCXO's). Unlike quartz, the MEMS resonators used here do not suffer much from stress-

induced frequency shifts, but are instead limited more by an electrical stiffness effect.

II. Acceleration–Induced Oscillator Frequency Instability

The procedure for measurement of oscillator acceleration sensitivity essentially entails vibrating the oscillator at frequency f_v, while measuring its output spectrum. In such a scheme the ratio between the induced sideband and carrier powers shown in Fig. 1 can be expressed as [3]

$$\mathcal{L}(f_v) = 20\log\left(\frac{(\vec{\Gamma}\cdot\vec{a})\cdot f_0}{2f_v}\right) \text{ with } \frac{\Delta f}{f_0} = \vec{\Gamma}\cdot\vec{a} \quad (1)$$

where f_0 is the oscillation frequency, $\vec{a}$ is the peak amplitude of the acceleration vector, and $\vec{\Gamma}$ is the acceleration sensitivity vector of the oscillator gauging fractional changes in oscillation frequency due to a unit g acceleration. In the presence of random vibration, this noise would appear as $1/f^2$ phase noise.

The acceleration sensitivity vector can be described in a Cartesian coordinate system fixed to the resonator by

$$\vec{\Gamma} = \Gamma_x\,\overrightarrow{a_x} + \Gamma_y\,\overrightarrow{a_y} + \Gamma_z\,\overrightarrow{a_z} \text{ and } |\vec{\Gamma}| = \sqrt{\Gamma_x^2+\Gamma_y^2+\Gamma_z^2} \quad (2)$$

where $\overrightarrow{a_x}$, $\overrightarrow{a_y}$, and $\overrightarrow{a_z}$ are peak acceleration vectors in different directions, and $|\vec{\Gamma}|$ is the magnitude of their vector sum. It is this vector sum that is normally used to compare oscillator performance. For quartz crystal oscillators, $|\vec{\Gamma}|$ may vary from $5\times10^{-11}/g$ [4] to $10^{-7}/g$ [5] depending on crystal design, cut, mounting, and whether or not feedback compensation circuits (that normally use accelerometers) are employed. As might be expected, the lower the acceleration sensitivity, the much more expensive the oscillator.

III. Device Operation and Oscillator Design

The wine-glass disk resonator used in this work consists of a 3µm-thick, 32µm-radius polysilicon disk supported at nodal points by four beams and surrounded by electrodes spaced only 92nm from its edges, as shown in Fig. 2. To excite the resonator, a bias voltage V_P is applied to the disk and an ac drive voltage to the input electrode. These voltages combine to produce a force across the input electrode-to-resonator gap that drives the resonator into the wine-glass (i.e., compound (2, 1)) mode shape, which comprises expansion and contraction of the disk along orthogonal axes. This occurs when the input frequency matches the wine-glass mode resonance frequency given by [6]

$$f_{nom} = \frac{K}{R}\sqrt{\frac{E}{\rho(2+2\sigma)}} \quad (3)$$

where R is the disk radius, K = 0.373 for polysilicon structural material, and E, σ, and ρ are Young's modulus, Poisson ratio, and density of the structural material, respectively.

As shown in Fig. 3, the transimpedance amplifier is similar to that used in [2] and consists of a fully differential

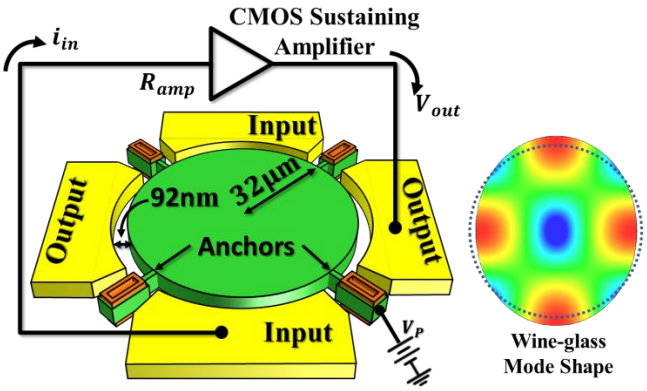

Fig. 2: Perspective-view schematic of a micromechanical wine-glass disk resonator (with mode shape shown to the right) embedded in a positive feedback with a sustaining amplifier to form a self-sustained oscillator.

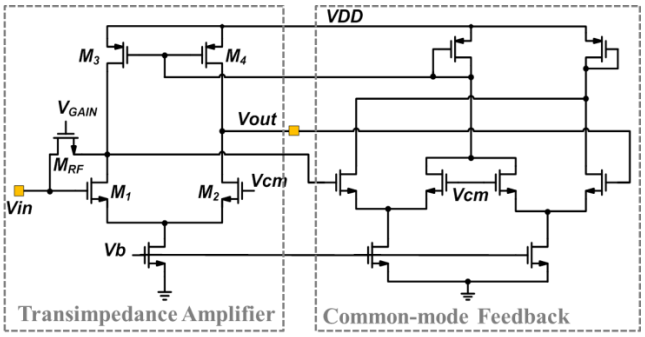

Fig. 3: Schematic of the transimpedance amplifier employing differential design and common-mode feedback to reject common-mode noise, including that introduced by vibration.

CMOS amplifier connected in shunt-shunt feedback on one side, with output taken from the other side to realize a 0° phase shift from input to output. The value of resistance in the shunt-shunt feedback loop sets the total closed-loop transimpedance gain of the amplifier. Transistors, M_1-M_4, comprise the basic differential pair biased by a common-mode feedback circuit that preserves low output resistance and cancels out common-mode noise, including that caused by vibration. The MOS transistor M_{RF} is biased in the triode region to serve as a voltage controllable shunt-shunt feedback resistor that allows convenient adjustment of the TIA gain via its gate voltage, V_{GAIN}.

The amplifier IC was fabricated in a 0.35µm CMOS technology. Although the entire die, shown in Fig. 4, occupies an area of 900µm×500µm, the actual sustaining amplifier only consumes about 100µm×100µm. The rest of the area is consumed by 1) an on-chip buffer used to drive 50Ω measurement systems; 2) by-pass capacitors that further reduce noise, particularly caused by vibration, on DC supply lines; and 3) multiple bond pads. The amplifier die is bondwired to the resonator and package, as also shown in Fig. 4, to yield the oscillator under test.

IV. Resonator Acceleration Sensitivity

Among possible mechanisms that give rise to accelera-

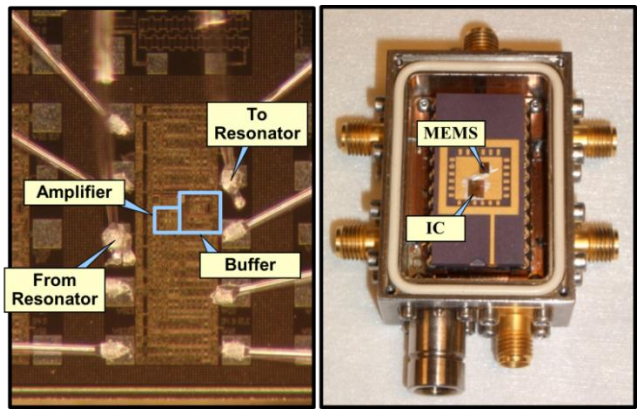

Fig. 4: Left: die photo of custom-made transimpedance amplifier. Right: photo of the oscillator in a custom-designed vacuum box.

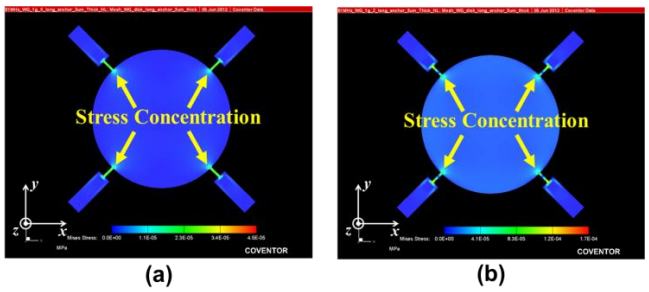

Fig. 5: Finite Element Simulation (FEM) of the resonator subjected to (a) lateral acceleration and (b) vertical acceleration, showing stress concentrations in the structure.

tion-induced resonance frequency shifts in the wine-glass disk of this work, two stand out: 1) acceleration-induced mechanical stress, which is historically the main mechanism in quartz crystals; and 2) acceleration-induced changes in electrical stiffness, which is somewhat new and unique to capacitive-gap transduced MEMS-based resonators.

A. Mechanical Stress-Induced Frequency Instability

When the disk undergoes acceleration, its anchored support beams introduce stresses into its structure that then change its resonance frequency. Because the wine-glass disk is orders of magnitude smaller than a typical quartz crystal, its inertia is also many times smaller. Moreover, its support beams are strategically designed to attach to the disk at nodal points of the wine-glass mode shape. As shown in Fig. 5, this concentrates any acceleration-induced stress to nodal points in the vibration mode shape, where their influence on the resonance frequency of the disk is minimal. Finite element simulation using nonlinear models in Coventorware predicts $|\vec{\Gamma}| = 5\times10^{-14}/g$. Of course, since computer simulation is not infallible when it comes to predicting values this small, these specific numbers are perhaps best taken with a grain of salt, with the main take-away being not the specific numbers, but that mechanical-stress induced acceleration sensitivity is very small for the anchor-isolated MEMS-based resonator used here.

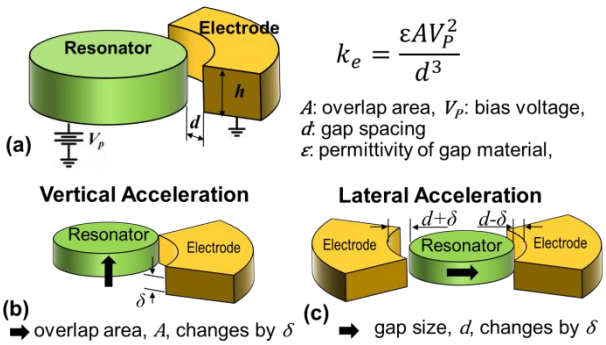

Fig. 6: (a) Schematic of the resonator along with the electrical stiffness formula. (b) Overlapping area and (c) gap spacing change when the resonator experiences vertical and lateral acceleration, respectively.

B. Electrical Stiffness-Induced Frequency Instability

If mechanical stresses are too small for this device on this scale, then perhaps the dominant mechanism for acceleration sensitivity involves the electrical stiffnesses generated across the tiny electrode-to-resonator gaps in Fig. 2. In particular, when the disk vibrates, cf. Fig. 6(a), the gap spacing between it and its electrode changes, which in turn means the electric field in the gap varies. It follows that the electrostatic force in the gap must also change, and it does so in phase with the disk edge displacement and with a magnitude that is proportional to it. Since any mechanism that generates a force in phase with and proportional to displacement fits the definition of stiffness, this electrical field-dependent phenomenon is popularly termed the electrical stiffness and can be expressed as [8]

$$k_e = \frac{\varepsilon A V_P}{d^3} \tag{4}$$

where ε is permittivity of the gap material (i.e., vacuum in this case), A is the overlap area between the resonator and its electrodes, and d is the gap spacing between them.

Since the electrostatic force aids the motion of the resonator, this electrical stiffness actually softens the total stiffness of the structure and therefore reduces the resonance frequency as described by

$$f_0 = f_{nom}\sqrt{1-\left\langle \frac{k_e}{k_m} \right\rangle} \tag{5}$$

where f_{nom} is the nominal resonance frequency defined purely by geometry (with no applied voltages), and $\langle k_e/k_m \rangle$ is the integrated ratio of electrical stiffness to mechanical stiffness k_m [9]. If external vibration induces a change in k_e, the corresponding change in resonance frequency can be approximated (when the change is small) as

$$\frac{\Delta f}{f_0} \cong -\frac{1}{2}\frac{\Delta k_e}{k_m} \tag{6}$$

For the case where the disk experiences a vertical acceleration, the height of its electrode-to-resonator overlap area changes by δ, as shown in Fig. 6(b). According to (4), the change in k_e due to a change in overlap area, ΔA, can be

expressed as

$$\Delta k_{e,z} = k_e \frac{\Delta A}{A} \tag{7}$$

Coventorware finite element simulation predicts for the 61-MHz wine-glass disk used in this work a change in overlap area per unit acceleration, g, in the z-direction of ΔA=3.722×10^{-6}μm^2/g. Substituting this number into (7), and combining with (1) and (6), the corresponding z-direction acceleration sensitivity $\Gamma_{z,ke}$ component is

$$\Gamma_{z,ke} = 5.76\times10^{-13}/g \tag{8}$$

For the case where the disk experiences a lateral acceleration, its electrode-to-resonator gap spacings change. Similar to the vertical case, the change in k_e due to a change in gap, Δd, can be approximated using the first two terms of the Taylor series expansion of (4) as follows

$$\Delta k_{e,x} = \Delta k_{e,y} \cong k_e\left(-3\frac{\Delta d}{d} + 6\cdot\left(\frac{\Delta d}{d}\right)^2\right) \tag{9}$$

If the disk of Fig. 2 had only one electrode covering one quadrant of its sidewall area, then the frequency shift imposed by (6) could actually be significant. However, the disk of Fig. 2 sports not just one, but four electrodes placed symmetrically around its perimeter. In this scheme, if the gap decreases by δ on the right side of the disk, as shown in Fig. 6(c), a corresponding gap increase by δ ensues on the left side. The total change in Δk_e is the sum of Δk_e^+ due to a gap decrease and Δk_e^- due to a gap increase:

$$\Delta k_{e,x} = \Delta k_{e,y} = \Delta k_e^+ + \Delta k_e^- \cong \frac{k_e}{4}\left(12\cdot\left(\frac{\Delta d}{d}\right)^2\right) \tag{10}$$

where k_e is divided by 4 because the wine-glass disk resonator has four electrodes. Coventorware simulation gives Δd=2.3285×10^{-6}nm/g, which then yields

$$\Gamma_{x,ke} = \Gamma_{y,ke} = 1.4978\times10^{-19}/g \tag{11}$$

This is far smaller than the already very small acceleration sensitivity due to electrical stiffness in the z-direction.

V. Experimental Results

The wine-glass disk resonators used for testing were fabricated via a previously described three-polysilicon self-aligned stem small lateral-gap process [10]. Fig. 7(a) presents the scanning electron micrograph (SEM) of a fabricated 61-MHz wine-glass disk resonator, while Fig. 7(b) shows a typical measured frequency response, where Q's of 130,000 in vacuum and motional impedances of 15kΩ at V_P=5V were common among devices.

A. Measurement Setup

To maintain high (i.e., over 50,000 loaded) resonator Q, and thereby minimize phase noise [1], the MEMS-based oscillator should operate in a stable vacuum environment during measurement. This is achieved via a custom-made

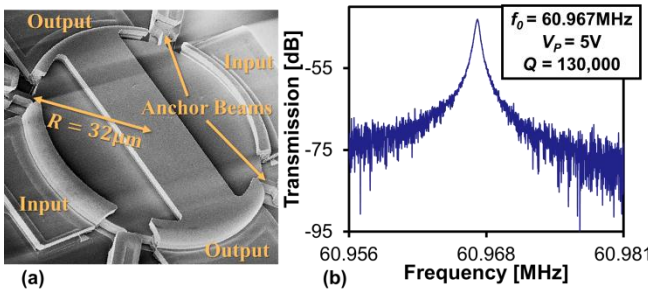

Fig. 7: (a) SEM of a fabricated wine-glass disk resonator. (b) The measured frequency response of the wine-glass disk resonator.

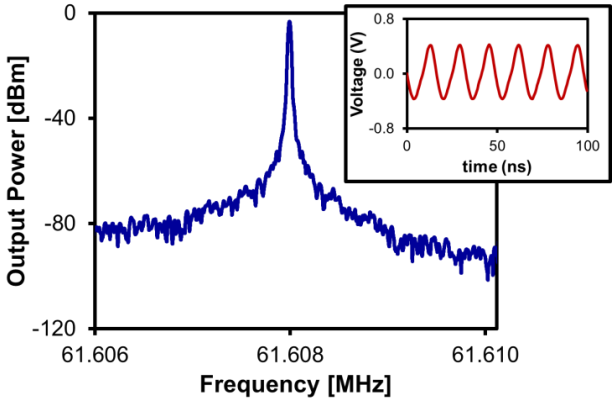

Fig. 8: The measured output power spectrum of the wine-glass disk oscillator. Inset: its measured output waveform.

miniature vacuum chamber, shown in Fig. 4, containing a printed circuit board (PCB) board that houses the MEMS/CMOS device package and provides electrical feedthroughs to allow connection to outside instrumentation. Once sealed, this system provides weeks to months of measurement time under at least a 20Torr vacuum, which is sufficient to support Q's >50,000 for wine-glass disks. Fig. 8 presents the measured output power spectrum of the MEMS-based oscillator operating inside this chamber.

B. Parasitic Acceleration Sensitivity

Unfortunately, the device of interest is often not the only component in an acceleration sensitivity test setup that responds to acceleration. Indeed, the electronic components, the PCB, and the wires and solder joints, are all also sensitive to acceleration due to stress, as well as to charge distribution and electromagnetic interference. The measurement system shown in Fig. 9 constructed around an ET-139 shaker table from Labworks Inc. pays careful attention to these noise contributors. In this setup, the vacuum box housing the MEMS-based oscillator is securely bolted onto the shaker table in one of the three orthogonal orientations. A low-noise analog voltage regulator board supplies all needed bias and supply voltages to the amplifier via shielded coaxial cables routed through weighed foam pads for vibration isolation and away from the power amplifier driving shaker table. A single coax line carries the oscillator output waveform for capture of output spectra on a N9030A Agilent

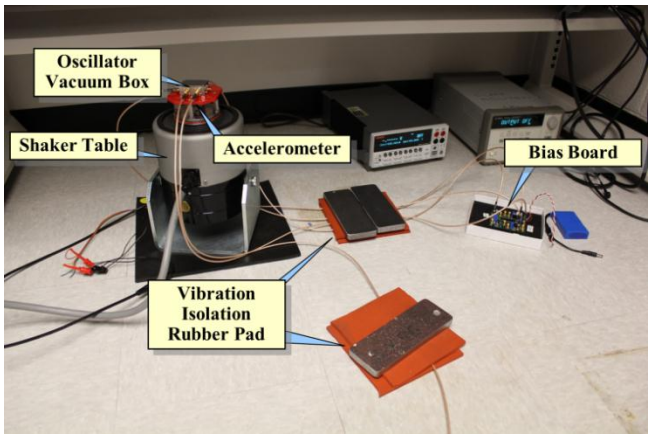

Fig. 9: Acceleration sensitivity measurement setup.

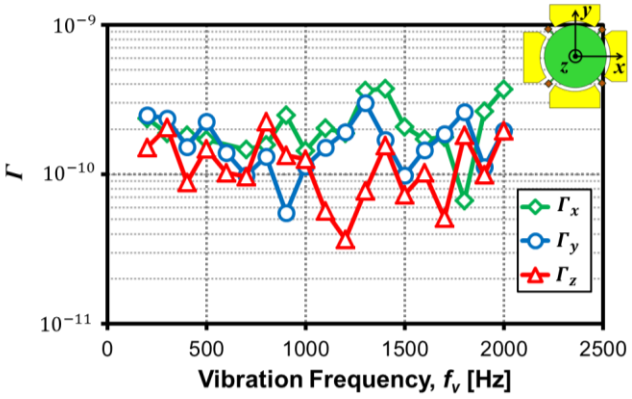

Fig. 10: Plot of measured Γ components versus vibration frequency.

spectrum analyzer. This setup incorporates many improvements over that used in [7], including removal of acceleration sensitive components from the accelerated PCB and simplification of the feedback loop from large PCB-level wires to short die-level bondwires.

To apply acceleration, the shaker table is driven by a variable-amplitude sine wave at frequencies from 100Hz to 2kHz. An ADXL326Z accelerometer from Analog devices mounted directly beneath the oscillator senses the amplitude of acceleration, converting it to an electrical signal that then feeds a Stanford Research Systems SR830 lock-in amplifier. This setup provides a highly accurate and noise-free measure of acceleration amplitude at the frequency of interest.

C. Measurement Results

Using the refined experimental setup, the acceleration sensitivity of the packaged oscillator of Fig. 4 was measured in all three orthogonal directions up to 2kHz. Fig. 10 presents all measured gamma components and demonstrates a remarkable sensitivity Γ~0.2ppb/g in all directions at all measured frequencies. This value is at least a factor of ~30x better than the work of [7], cf. Fig. 11, and marks the best performance posted to date for a MEMS-based oscillator, cf. Fig. 12, outperforming even those enhanced by accelerometer-based feedback compensation circuits [11][12].

To provide a comparison to commercial quartz devices

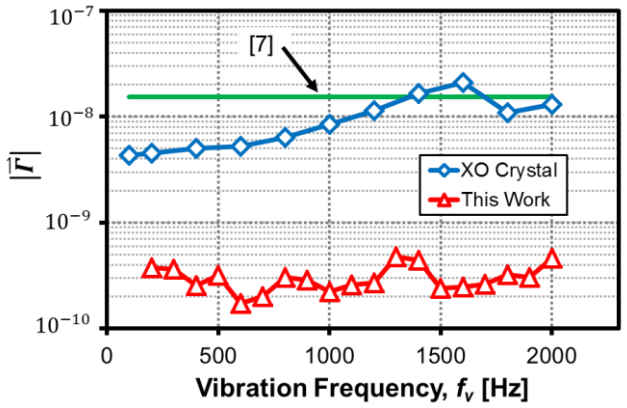

Fig. 11: Plot of measured Γ vector sum versus vibration frequency for the 61-MHz micromechanical disk oscillator alongside similar plots for previous work using a similar resonator device and a measured 66.67-MHz off-the-shelf crystal oscillator.

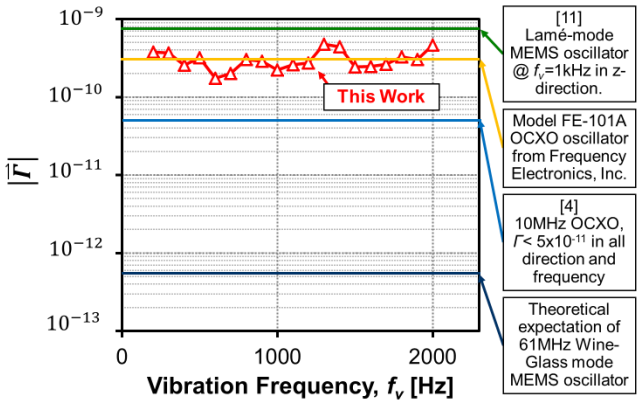

Fig. 12: Plot of Γ vector sum versus vibration frequency for the 61-MHz micromechanical disk oscillator alongside lines indicating the performance of oscillators in the literature and that of the theoretical expectation.

and as an additional qualification of the measurement system, several "off-the-shelf" 66.67MHz quartz oscillators were measured as direct drop-in replacements for the bondwired MEMS oscillator inside the hermetic vacuum box. Fig. 11 compares the measured Γ-vector sum of one of these oscillators with that of the MEMS oscillator, as well as with the work of [7]. As shown, the MEMS oscillator measured via the improved system displays more than an order of magnitude reduction in sensitivity over the commercial quartz. While this is not the best quartz can do—bulky, high-cost quartz oscillators built explicitly for acceleration insensitivity are significantly better—this does represent a fair comparison to a low-price, high-volume product. Even though the MEMS oscillator is not as good as one of the best crystal oscillators measured [4] shown in Fig. 12, it certainly outperforms generic quartz and is even on par with most (expensive) low sensitivity OCXO's, laying to rest, and in fact reversing, concerns that MEMS-based oscillators are intrinsically worse than quartz alternatives.

Despite these impressive performance numbers, measured sensitivities still fall short of that predicted by the theo-

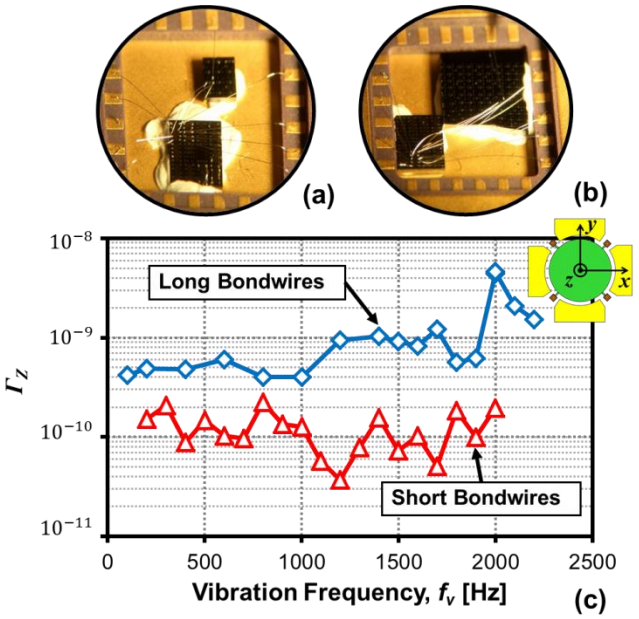

Fig. 13: Photos of oscillators: (a) using short bondwires and (b) using long bondwires, particularly those connecting to the resonator dc-bias V_P and the input/output of the amplifier. (c) Plot of measured Γ_Z of these oscillators versus vibration frequency.

ry of Section IV for the MEMS device itself. Indeed, although many precautions were taken to eliminate extraneous sources of vibration noise, some still remain, particularly bondwires. The influence of bondwires was further explored by constructing and measuring an additional oscillator with intentionally lengthened bondwires, particularly those within the oscillation loop linking the amplifier to the MEMS resonator, and one connected to the resonator dc-bias voltage V_P. Fig. 13(a) and (b) present close-up photos of both oscillators, showing the much longer bondwires of design (b). Fig. 13(c) presents the measured data, showing close to an order of magnitude decrease in *z*-direction sensitivity for the device with short versus long bondwires at all frequencies measured.

These results strongly suggest that flexing wires on sensitive nodes constitute a primary limitation on past, and possibly present, measurements. While the exact nature of the coupling of bondwire motion to the oscillation frequency is not precisely known, inductive and capacitive effects could easily explain it. Additionally, the spikes seen in the measured acceleration sensitivity versus frequency curve of Fig. 13(c) can be well understood as weak mechanical resonances in the bondwires themselves.

VI. Conclusions

The acceleration sensitivity of a 61-MHz vibrating wine-glass disk resonator is measured to be at least as good as Γ ~0.2ppb/g for vibration frequencies up to 2kHz and in all directions, yielding a vector-sum magnitude $|\vec{\Gamma}|$ less than 0.5ppb/g. This remarkable number is achieved without any compensation and marks the best among MEMS-based oscillators, including those aided by accelerometer-based feedback compensation circuits. It is more than an order of magnitude better than an off-the-shelf crystal oscillator and is now comparable with some low sensitivity OCXO's.

However, the measured acceleration sensitivity is still about two orders of magnitude worse than the theoretical expectation for the MEMS device itself, and there is evidence that the current measurement setup bondwires are a primary limitation. This motivates the use of more fully integrated systems, such as flip-chip or MEMS-last fabrication of resonators on CMOS, to achieve even better results.

Nevertheless, the low sensitivity to environmental vibration exhibited by a tiny uncompensated MEMS-based oscillator is already impressive enough to alleviate concerns in some minds that MEMS-based oscillators are intrinsically worse than quartz alternatives and should enable a myriad of harsh environment applications where both stable and compact reference oscillators are required.

References

[1] D. B. Leeson, "A simple model of feedback oscillator noise spectrum," *Proceedings of the IEEE*, vol. 54, no. 2, pp. 329 – 330, Feb. 1966.

[2] Y.-W. Lin, S.-S. Li, Z. Ren, and C. T.-C. Nguyen, "Low phase noise array-composite micromechanical wine-glass disk oscillator," *Technical Digest, IEEE Int. Electron Devices Mtg.*, Washington, DC, Dec. 5-7, 2005, pp. 287-290.

[3] R.L. Filler, "The acceleration sensitivity of quartz crystal oscillators: a review," *IEEE Trans. on Ultrasonics, Ferroelectrics and Frequency Control*, vol. 35, no. 3, pp. 297-305, May 1988.

[4] D.A. Howe, J.L. LanFranchi, L. Cutsinger, A. Hati, and C. Nelson, "Vibration-induced PM noise in oscillators and measurements of correlation with vibration sensors," in *Proc. IEEE Int. Frequency Control Symposium and Exposition*, 2005, pp., 494-498, Aug. 2005.

[5] J.R. Vig, "Quartz crystal resonators and oscillators for frequency control and timing applications – a tutorial," Apr. 2012.

[6] M. Onoe, "Contour vibrations of isotropic circular plates," *J. Acoust. Soc. Amer.*, vol. 28, no. 6, pp. 1158–1162, Nov. 1956.

[7] B. Kim, M. Akgul, Y. Lin, W.-C. Li, Z. Ren, and C. T.-C. Nguyen, "Acceleration sensitivity of small-gap capacitive micromechanical resonator oscillators," *IEEE Int. Frequency Control Symposium (FCS)*, pp.273-278, 1-4 June 2010.

[8] H.C. Nathanson, W.E. Newell, R.A. Wickstrom, and J.R. Davis Jr., "The resonant gate transistor," *IEEE Transactions on Electron Devices*, vol.14, no.3, pp. 117- 133, Mar. 1967.

[9] Y.-W. Lin, S. Lee, S-S Li, Y. Xie, Z. Ren, and C.T.-C. Nguyen, "Series-resonant VHF micromechanical resonator reference oscillators," *Solid-State Circuits, IEEE Journal of* , vol.39, no.12, pp. 2477- 2491, Dec. 2004

[10] M. A. Abdelmoneum, M. U. Demirci, and C. T.-C. Nguyen, "Stemless wine-glass-mode disk micromechanical resonators," in *Micro Electro Mechanical Systems, 2003. MEMS-03 Kyoto. IEEE The Sixteenth Annual International Conference on*, 2003, pp. 698 – 701.

[11] B. Kim, R.H. Olsson, K. Smart, and K.E. Wojciechowski, "MEMS resonators with extremely low vibration and shock sensitivity," *IEEE Sensors*, pp.606-609, 28-31 Oct. 2011.

[12] S. Yoneoka, J. C. Salvia, G. Bahl, R. Melamud, S. A. Chandorkar, and T. W. Kenny, "Active electrostatic compensation of micromechanical resonators under random vibrations," *Microelectromechanical Systems, Journal of*, vol. 19, no. 5, pp. 1270 –1272, Oct. 2010.